REVIEW

Fuel Cells DOI: 10.1002/fuce.200800034

Opportunities and Challenges in Materials Development for Thin Film Solid Oxide Fuel Cells

S. J. Litzelman[1], J. L. Hertz[1a], W. Jung[1], H. L. Tuller[1]*

[1] Department of Materials Science and Engineering, Massachusetts Institute of Technology, 77 Massachusetts Ave., Cambridge, MA 02139, USA

Received May 06, 2008; accepted June 25, 2008

Abstract

Solid oxide fuel cells (SOFCs) are currently the focus of intense investigation given their high chemical-to-electrical energy conversion efficiency and low carbon footprint. In this review, the development of thin film SOFCs, sometimes described as 'micro-SOFCs', is highlighted and analysed. Opportunities for reduced temperature operation and portable power generation arise from the decreased thickness of the solid electrolyte, as well at the metastable phases and nanoscale-dependent effects that are a consequence of the reduced temperature of fabrication. Challenges such as enhanced cation diffusion along grain boundaries are; however, also observed, potentially impacting the long-term stability of these devices. Recent progress achieved in understanding these and other challenges are reviewed and directions for future work identified.

Keywords: Grain boundary diffusion, Micro-SOFC, Nanoionics, Phase stability

1 Introduction

Solid oxide fuel cells (SOFCs), based on the use of oxygen ion conducing ceramic membranes, are currently the focus of intense investigation as a direct chemical-to-electrical energy conversion technology given their high conversion efficiency and low carbon footprint. Historically, the majority of materials development for SOFC research and applications has taken place in the form of bulk ceramics and thick films. However, recent trends indicate an increasing interest in thin film SOFC components, particularly for the solid electrolyte layer. This trend is driven by several technological objectives. One is the desire to decrease the operating temperature of SOFCs from the current range of 800–1,000 °C, to an 'intermediate' temperature range of 600–750 °C. These operating temperatures enable the use of lower-cost metallic interconnects and reduce the thermal stresses and reaction products, yet still remain high enough to retain fuel flexibility [1]. Reduced temperatures, however, lead to increased electrolyte ohmic resistance losses, given the thermally activated behaviour of ionic transport [2]. This effect can, however, be compensated by decreasing electrolyte thickness. For example, for an area-specific resistance (ASR) of 0.15 Ω-cm^2, the decrease in thickness of a 10 mol% yttria-stabilised zirconia (YSZ) electrolyte from 15 μm to 500 nm allows for a reduction in operating temperature from 700 °C to approximately 525 °C [3]. A number of research efforts have been directed towards studying the properties of thin film electrolytes and, to a lesser extent, electrodes and incorporating them into SOFC devices.

A second major driving force for thin film SOFCs is the development of micro-SOFCs for portable power generation in devices such as laptop computers and mobile telephones [4–7]. The most appealing benefit over batteries is longer usage time between recharges, given the considerably greater energy density of liquid fuels than that of state-of-the-art batteries. In contrast to large-scale fuel cell stacks that output power on the order of megawatts, these micro-devices are intended to produce power on the order of milliwatts to

[a] *Current address: National Institute of Standards and Technology, 100 Bureau Drive, MS8362, Gaithersburg, MD 20899, USA.*

[*] *Corresponding author, tuller@mit.edu*

several watts. As noted by Nikbin, researchers in the US, Europe and Japan are in the preliminary stage of addressing the major issues of micro-SOFC devices and assembling prototypes [6].

In this paper, recent results related to thin film SOFC materials development and characterization, including recent work from the authors' laboratory, are summarized. Implications related to the use of thin, nanocrystalline films are emphasised.

2 Thin Nanostructured Solid Electrolytes

2.1 Thermomechanical Effects

Production of *thin film* micro-fuel cells *typically* requires the formation of a freestanding thin film 'stack' so that the fuel and oxidant gases can access both the anode and cathode (we are excluding from consideration 'micro-SOFCs' that are produced using more conventional ceramic processing routes, e.g. [8]). Since the power output is proportional to the area of exposed electrode, a freestanding membrane with an area as large as possible is desired. Conversely, the thermomechanical stability of the membrane generally favours smaller membranes. Therefore, a balance between power output and stability must be reached [9].

Despite the apparent difficulties, a number of research groups have successfully created large area, freestanding thin film ceramic membranes [7, 10–12]. Bieberle-Hütter et al. reported fabrication of micro-SOFC stacks with free-standing membranes up to 5 mm in diameter supported on a Ni grid [13]. An open circuit voltage of 1.06 V and power output of 150 mW cm^{-2} at 550 °C were reported for single stacks. MIT researchers recently reported on the production and thermomechanical characterization of membranes composed of either YSZ or gadolinium-doped ceria (GDC) [4]. Films were deposited on single crystal silicon substrates that were subsequently removed in defined patterns using a two-stage etch process. Though comprising films only 100–1,000 nm thick, membranes as large as 1,025 μm^2 were obtained and survived annealing to 500 °C. As evidenced by changes in the shape of the membranes from buckled to taut, significant evolution in the film stresses occurred during annealing [14]. Thin film SOFC structures containing YSZ and YSZ/doped ceria multilayer electrolyte membranes of 50–150 nm thick and 80 nm porous Pt cathodes and anodes were reported by Huang et al. [15]. Individual cell areas as large as 240 × 240 μm^2 were successfully fabricated, and peak power densities of 200 and 400 mW cm^{-2} at 350 and 400 °C, respectively were reported.

Despite these successes, further work remains in improving the mechanical stability of the membranes to longer times and higher temperature. To improve the thermomechanical reliability, the causes of the residual stresses and stress evolution in the films must be determined [14]. These concerns may also be mitigated by incorporating stress tolerant designs (see, for example, Figure 1 and ref. [16]).

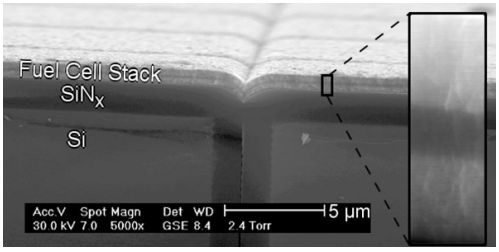

Fig. 1 SEM of the cross-section of a micro-fuel cell stack. The anode/electrolyte/cathode stack is shown magnified in the box. Pt-YSZ composite films are the light grey films on the top and bottom of the stack and YSZ is the darker grey film in between. The stack is deposited upon a silicon substrate into which silicon nitride support structures have been created. For use, all of the silicon and the horizontal sections of the silicon nitride must be removed to allow gas access to both anode and cathode. The vertical sections of silicon nitride would remain and provide mechanical support.

Chemical strain effects in ceramic thin films have recently been studied. Lubomirsky and co-workers reported the stress relaxation behaviour in a self-supported GDC membrane [17, 18]. Based on a deflection measurement of buckling in the thin film using atomic force microscopy (AFM), the authors concluded that a residual film stress can be modified by generation or elimination of defect associations in a reversible manner. Mandowara and Sheldon also studied stress evolution using an *in situ* wafer curvature technique during oxidation and reduction of CeO_2 thin films [19]. Those findings implied that a relaxation process through chemical interactions might be utilised to minimise the residual stress in the film and enhance the mechanical stability. Overall, it has become evident that the mechanical properties of thin films can have a direct impact on physical properties such as defect concentration and oxygen nonstoichiometry, which may lead to variations in electrical and electrochemical performance. This area of study thus merits sustained attention for future SOFC materials development

2.2 Nanostructural Effects

2.2.1 Grain Boundary and Interfacial Contributions

In addition to the thinness of the electrolyte layers, given the reduced processing temperatures, the grain size of such films is typically on the order of tens of nm. This size range is notable for its 'nano-ionic' effects, in which electronic and ionic charge transport can vary greatly from that in the bulk [20–22]. Often, these effects are due to the introduction of space charge regions, which are enhanced/depleted in mobile charge carrier concentration in response to segregation of charged defects/impurities to the grain boundary cores [23–25]. While nano-ionic effects have been observed [26] and modeled [27, 28] in simplified model systems such as CeO_2, evidence for such effects in practical electrolytes remains mixed. Indeed, the evidence for nano-ionic effects in YSZ is contradictory, with e.g. Kosacki et al. reporting substantial *increases* in ionic conductivity [29], whereas Peters

et al. report *decreases* in conductivity with decreasing grain size [30]. Mondal and Hahn prepared nanocrystalline 2–3 mol% YSZ, beginning with powders processed by the inert gas condensation technique, followed by sintering [31]. No significant changes from microcrystalline bulk properties were observed. Jiang et al. [32] published similar conclusions. In that study, ultra-fine grained YSZ was prepared by combustion synthesis using metal nitrates as precursor, followed by sintering. Consistent with refs. [30–32], a recent study of oxygen diffusion in nanocrystalline YSZ found no enhancement along the grain boundaries [33]. Given a lack of consensus, further exploration of nano-ionic effects in SOFCs is warranted. Below, the implications of nano-ionics for micro-SOFC development are presented and evaluated.

Unique nanocrystalline grain size effects on mixed ionic–electronic conductivity (MIEC) in oxide electrolytes, namely CeO_2, were first observed by Chiang et al. [26]. A decrease in grain size from 5 μm to 10 nm resulted in an orders of magnitude increase in electronic conductivity, reflected also in a shift from p_{O_2} independence of the electrical conductivity in the microcrystalline form to a strongly n-type p_{O_2} behaviour in the nanocrystalline form. This change in p_{O_2} dependence indicates a shift of the dominant charge transport mechanism from ionic to n-type electronic. These observations were later verified by Tschöpe [27] and by Kim and Maier [28], who successfully modeled charge transport in nanocrystalline ceria in terms of a space charge model. Namely, a positive electrostatic potential in the grain boundary core is compensated by negative space charge regions on either side of the boundary. These space charge regions, enhanced in electrons and depleted of oxygen vacancies, comprise a large enough fractional volume of the electrolyte to alter the observed electrical properties.

Suzuki et al. also examined the grain size effect in nanocrystalline CeO_2 [34] and GDC with 10 and 20% Gd on the Ce site [35]. While the electrical conductivity for CeO_2 with a grain size of 20 nm displayed n-type semiconductor behaviour near ambient p_{O_2}, in agreement with the data in ref. [26], nanocrystalline GDC displayed ionic behaviour in the p_{O_2} range of 10^{-5}–1 atm and for temperatures from 600 to 900 °C [35]. This behaviour is not surprising given the much higher oxygen vacancy density (relative to electron concentration) in the non-depleted regions as well as the much reduced Debye screening length given by

$$\lambda = \left(\frac{\varepsilon_o \varepsilon_r kT}{2z^2 e^2 c_\infty}\right)^{1/2} \quad (1)$$

where ε_o is the permittivity of free space, ε_r the relative dielectric constant, z the charge magnitude, e the elementary charge and c_∞ is the bulk majority defect concentration. For an electrolyte such as 8 mol% YSZ, the Debye length at 500 °C is estimated to be only ~1 Å. When considering the shape and spatial extent of space charge profiles, appropriate boundary conditions must be stated. In the temperature range of 600–750 °C, where IT-SOFCs are expected to operate, it is often assumed that the acceptor dopant (Y in YSZ) is not sufficiently mobile to redistribute under the influence of local electric fields [28, 36]. Under such Mott–Schottky boundary conditions, the depletion width is given as [37]

$$\lambda* = \left(\frac{2\varepsilon_o \varepsilon_r \Delta\varphi(0)}{z_j e c_{j\infty}}\right)^{1/2} = \lambda\left(\frac{4z_j e}{kT}\Delta\varphi(0)\right)^{1/2} \quad (2)$$

Using a value of 0.25 V for the space charge potential in 8 mol% YSZ [36], the depletion width λ* is expected to be approximately 4 Å at 500 °C. While four times larger than the Debye length, this calculated depletion width remains too small to induce a measurable shift from ionic to electronic conduction in YSZ, in agreement with studies in which electronic conduction in YSZ was not observed [29, 30].

A similar argument may be used to support the apparent lack of an ionic-to-electronic transition near ambient p_{O_2} in GDC [35]. Interestingly, the authors of ref. [35] did report an increase in the total conductivity and decrease in the activation energy with decrease in grain size. This observation is supported by the work of Rupp and Gauckler, who fabricated CeO_2 and GDC by PLD (x = 0.25) and spray pyrolysis (x = 0.22) [38]. In that work, decreasing the grain size of the thin film specimens also led to higher conductivity and lower activation energies. Due to the high acceptor doping content, these observations are unlikely to be explained by space charge effects. Indeed, the origin of the grain size-dependent conductivity and activation energy in GDC remains unclear.

Nano-ionic effects have also been reported at heterojunction interfaces. Sata, et al. reported that the ionic conductivity in artificially modulated planar heterostructures, composed of molecular beam epitaxy prepared alternating films of CaF_2 and BaF_2, exhibited considerably enhanced fluorine ion conduction as compared to individual CaF_2 or BaF_2 films [39]. The conductivity, measured parallel to the interfaces, was found to increase with decreased film thickness confirming fluorine ion accumulation/depletion respectively on the CaF_2 and BaF_2 sides of the interface, respectively. Guo et al. examined the lateral conductivity in the heterostructures as a function of inverse layer thickness, and concluded that the experimental results were best-described by a modified Mott–Schottky model, in which a gradient of the majority impurity, boron, is assumed to exist near the layer interface [40]. The authors attributed the conductivity enhancement to an increase of the defect $V_F^{\bullet}$ in the BaF_2 layer and F'_i in the CaF_2 layer, resulting in fast conduction in the BaF_2 layers due to the increased concentration of the high-mobility vacancies.

Other types of electroceramic multilayers have been demonstrated. Azad et al. fabricated structures consisting of alternating layers of GDC and ZrO_2 by plasma-assisted molecular beam epitaxy [41]. The electrical conductivity of the multilayers was increased relative to the end-members, and the peak conductivity was observed for a sample of ten layers. The authors concluded that, given the high Gd-doping concentration and a corresponding Debye length of ~1 Å, the conductivity increase could not be attributed solely to space

charge effects, as above. In a subsequent publication from the same laboratory, the conductivity enhancement was attributed to '. . .extended defects, interfacial misfit dislocations and the strain associated with the heterogeneity of the layer structures' [42]. Peters et al. examined the Ca-stabilised ZrO_2 (CSZ)–Al_2O_3 multilayer system, grown by pulsed laser deposition (PLD) [43]. The authors reported a structure of ten layers that was 60 times more conductive than bulk CSZ. A decrease in the activation energy for the ionic conduction was also observed with increase in number of interfaces. Similar to the ZrO_2/CeO_2 heterostructures, the Debye length was believed to be too small to contribute to the conductivity increase; rather, the authors assumed that a relationship between the decrease in activation energy and the structural disorder at the interface was the primary mechanism of enhanced conduction.

More directly relevant to this work, Kosacki et al. reported an enhancement in the ionic conductivity of 10 mol% YSZ thin films for film thicknesses of less than 60 nm [44, 45]. Given that these were epitaxial YSZ films deposited onto MgO substrates and that the enhancement of electrical conductivity occurred only for film thicknesses of less than 60 nm, the authors attributed the results to a highly conductive interfacial layer of approximately 1.6 nm thickness at the YSZ and MgO interface.

2.2.2 *Phase Stability Effects*

Ionic conduction is normally enhanced in solid oxide electrolytes by the addition of lower valent elements. Thus for YSZ, a double positively charged oxygen ion vacancy $V_O^{\bullet\bullet}$ is formed to charge compensate for every two single negatively charged Y ions, Y'_{Zr}, substituting on a Zr site. The defect reaction proceeds as

$$Y_2O_3 \xrightarrow{2ZrO_2} 2Y'_{Zr} + 3O_O^x + V_O^{\bullet\bullet} \tag{3}$$

The thermally activated ionic conductivity can be described by [46]:

$$\sigma_{ion} = \frac{\sigma_o}{T}\exp\left(-\frac{\Delta H_m}{kT}\right) \tag{4}$$

where σ_o is a temperature-independent constant equaling

$$\sigma_o = \frac{2e^2[Y'_{Zr}]D_o}{k}\exp\left(\frac{\Delta S_m}{k}\right) \tag{5}$$

where D_O is a temperature-independent constant relating to the oxygen vacancy jump process, k Boltzmann's constant and ΔS_m is the entropy of migration. For a given temperature, the above expression, appropriate in a dilute solution approximation, predicts that the ionic conductivity increases linearly with the Y dopant level. Instead, the ionic conductivity in cubic YSZ decreases monotonically with increasing Y content.

In the Y_2O_3–ZrO_2 system, this maximum occurs around 9 mol% Y_2O_3 ($x \sim 0.18$, see Fig. 2) [47]. This maximum corresponds to the minimum dopant level needed to stabilise the high-temperature cubic phase. For compositions beyond this point, the ionic conductivity decreases with increase in doping content. Models such as vacancy ordering and defect association have been proposed to describe this decrease [48, 49]. Recently, another model was proposed that suggested that the conductivity decrease was a result of a changing activation barrier in the atomistic jumping process, due to an enhanced fraction of Y–Zr edges through which the oxygen ion must jump [50]. Regardless of the exact mechanism, it is clear that excessive doping decreases the ionic conductivity due to reduced mobility of the ionic charge carriers.

Researchers have also studied the effects of nanocrystalline dimensions on phase stability. The tetragonal phase, which is normally stable only above 1,200 K, was observed to exist at room temperature in nanocrystalline undoped zirconia [51–53]. Other reports of metastable phases found in nanocrystalline materials such as alumina [54] and graphite [55] have also been published. Metastable phases have been detected in nanocrystalline YSZ thin films prepared by low-temperature sputtering. Kao [56] compared the properties of films produced on room temperature substrates by ion-beam sputtering from a pure Zr metal target and a YSZ target. Films produced from the oxide target consisted of a mono-disperse distribution of ~24 nm monoclinic crystallites in an amorphous matrix, despite the Y stabiliser in the target and, presumably, the film. After annealing, the films displayed a mixture of monoclinic and cubic phases. Films from the metal target were mostly amorphous, with a sparse distribution of extremely fine cubic crystallites. After annealing at 450 °C, these films were almost fully transformed into the cubic phase, which is quite unexpected for undoped zirconia. Jankowski and Hayes [57] reported that films grown with a low sputtering rate were fully oxidised and cubic, but films with a very high sputtering rate were oxygen deficient and contained an orthorhombic phase. Hobein et al. [58] sputtered a $Zr_{0.8}Y_{0.2}$ alloy target over a range of oxygen partial pressures and substrate temperatures from 500 to 700 °C. Pronounced

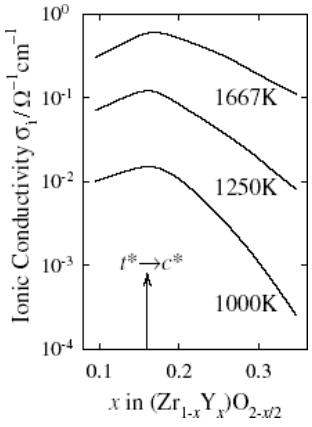

Fig. 2 Ionic conductivity of YSZ as a function of Y concentration, shown for three temperatures. The symbol t* → c* indicates the tetragonal to cubic phase transition [47].

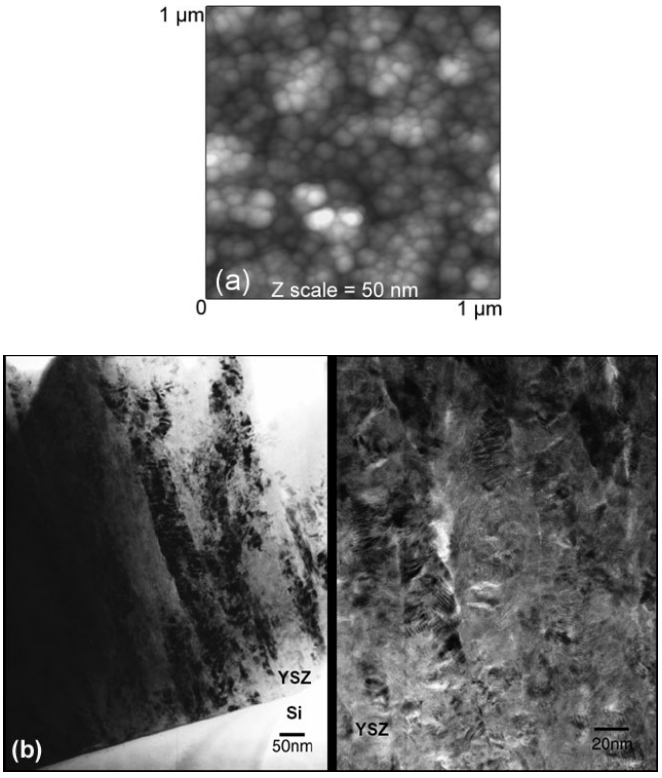

Fig. 3 (a) AFM and (b) TEM (cross-sectional and plan-view) micrographs of YSZ thin films, indicating a columnar microstructure and grain sizes on the order of 25–35 nm.

tetragonal phases in a cubic matrix were observed for samples grown at reduced oxygen partial pressures.

In research conducted in the authors' laboratory, nanocrystalline zirconia films were prepared with systematically varying *yttrium fraction* in order to better understand the relationship between composition, phase stability and ionic conductivity. YSZ films with yttrium levels between 0.5 and 8.7 mol% and 500 nm to 1 µm thickness were produced by reactive magnetron sputtering on amorphous, fused-silica substrates. Film microstructures were characterised by scanning electron microscopy (SEM), transmission electron microscopy (TEM) and AFM. As shown in Figure 3, the AFM image (a) shows the grain size to be approximately 25 to 35 nm and the TEM images (b) indicate columnar growth. Six different compositions of YSZ were deposited using high-purity yttrium–zirconium metal alloy targets. Dense platinum interdigitated electrodes were microfabricated on the surface of the YSZ thin films by a lithographic lift-off technique. A schematic and photograph of these microstructured electrodes are shown in Figure 4 [59].

Preliminary results suggested that high levels of ionic conductivity could be achieved in YSZ thin films with reduced levels of yttrium (W. Jung, J. L. Hertz, H. L. Tuller, unpublished). Following completion of impedance spectroscopy studies, it was determined that the peak conductivity in nano-YSZ shifted to the reduced Y concentration of ~6.4 mol%, rather than that found in bulk YSZ in the vicinity of 9 mol%. Second, the magnitude of that conductivity was 1 ~ 2 orders of magnitude greater than reported literature values for YSZ [60]. These results point to the feasibility of improving the ionic conductivity of YSZ at intermediate temperatures through nanostructuring, with promising implications for IT-SOFC design.

3 Nanocomposite Electrodes

Electrodes processed using traditional powder methods are thick, porous composites thereby providing a large triple phase boundary length *per* unit surface area l_{TPB}, accessible through the thickness. As shown in e.g. [61], the resistance of anodes and cathodes processed this way decrease as the thickness increases. Optimal values were only reached when the electrodes were greater than 10 µm in thickness. Thus, for activation polarization, there appears to be a significant geometric disadvantage to using thin film electrodes given reduced l_{TPB}. One possible solution is to use MIECs. Because these materials can conduct both ionic and electronic species, they effectively broaden the triple phase boundary zone to include the entire surface of the MIEC. Recent studies on thin film model (La,Sr)(Co,Fe)O_3–LSCF electrodes demonstrate that the electrode impedance of these mixed conductors is largely oxygen surface exchange controlled and highly dependent on DC bias [62]. Unfortunately, studies by the authors on lithographically defined (La,Sr)CoO_3–LSC electrodes deposited onto YSZ showed evidence of interface reactivity even at temperatures as low as 500 °C [63, 64]. Given the very thin dimensions of the active layers in such cells, such interactions take on an even more critical role with respect to performance and operating life.

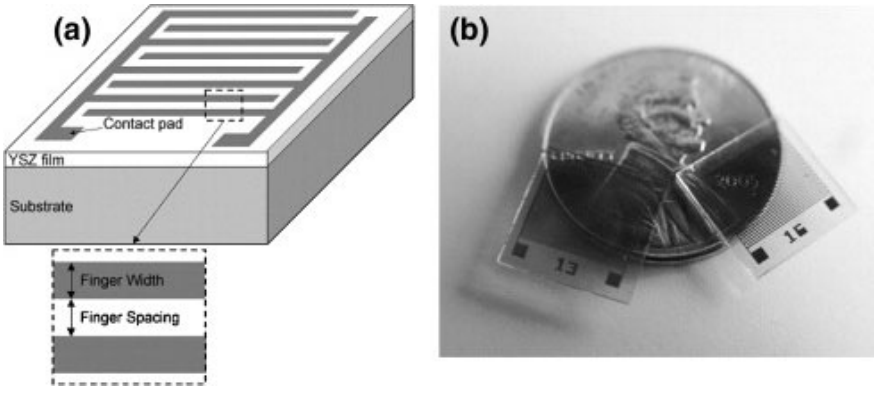

Fig. 4 Schematic (a) and photograph (b) of Pt dense microelectrodes on YSZ thin films on transparent substrates [59].

Another highly promising research direction to improve the performance of thin film SOFC electrodes is the use of nanocomposites. The *lTPB* should increase roughly in inverse proportion to the grain size of the components of an electrolyte/electronic conducting composite. Nanocomposites, with grain sizes in the range of 10–100 nm, thus hold the promise of vastly increased l_{TPB}, and thereby electrode performance. Physical vapour deposition (PVD) methods are a relatively straightforward method to produce such films, since the starting materials can be purified forms of the desired constituent phases of the nanocomposite [65–75]. A number of other deposition methods have also been successfully reported, including spray pyrolysis [76, 77], spin coating [78], and metallorganic chemical vapour deposition (MOCVD) [79]. Wang and Barnett have been particularly active in studying nanocomposites for SOFCs [69–73]. Key objectives for these production methods are to insure that mobile electrons and ions are both present at the triple phase boundaries and that a composite morphology exists exhibiting interpenetrating and mutually connected (i.e. bicontinuous) networks of electron and ionic conductors.

The very high chemical stability of platinum and YSZ allows for their use in both oxidizing and reducing environments. This capability allows a Pt-YSZ composite to be used as both the anode and cathode of a fuel cell. The authors recently reported on a Pt-YSZ nanocomposite produced by simultaneously co-sputtering from Pt and metal alloy Y/Zr targets [80]. A working pressure in the sputtering chamber of 10 mTorr, composed of either 90:10 or 95:5 Ar/O_2 was found to be sufficient to create fully oxidised YSZ. The Pt, as a noble metal, was not oxidised. Optimised deposition temperature and Pt to YSZ ratio resulted in the desired bicontinuous morphology. The electrode impedance measured in air was similar in magnitude to that expected from a dense, single-phase platinum electrode with as high a l_{TPB} as could be achieved only by sub-micron lithography.

One of the most problematic thermal stresses for a membrane is the bending moment created when there is a gradient in the thermal expansion coefficient through the thickness. This issue is avoided when the anode and cathode are the same material, as is possible with the Pt-YSZ nanocomposite electrodes (see Fig. 1). Using the electrolyte material within the nanocomposite further reduces thermal stresses by making the thermal expansion coefficient more uniform throughout the stack. None of these approaches, however, directly confronts what may be the largest source of thermal stresses: the mismatch in thermal expansion coefficient between the substrate and the fuel cell stack. The optimal selection of substrate and film materials for a micro-fuel cell will therefore remain as a key challenge.

The electrical performance of nanocomposite electrodes may be improved further by including porosity. This would allow fuel and oxidant access to the film interior, further increasing l_{TPB}. Other opportunities include the use of higher performance materials within the composites such as doped cerium oxides which have higher ionic conductivity than YSZ.

4 Cation Diffusion Along Grain Boundaries

In a recent review of materials for micro-SOFCs by Beckel et al. [7], various methods for fabrication of thin film solid electrolytes were discussed. Two of these approaches, sputter deposition and PLD, are broadly classified as PVD techniques, and are well-established methods for thin film fabrication. One major benefit of these techniques is that through judicious control of deposition parameters such as temperature, power and oxygen partial pressure, the microstructure and morphology of these films can be systematically controlled [81]. Often, thin films fabricated by these techniques display a columnar microstructure and nanocrystalline grain size. This microstructure is prevalent because the homologous temperature of deposition, T/T_m is often in the range of 0.2–0.4. In this range, the mobility of surface ad-ions is limited, and the surface kinetics may not be sufficiently fast to diffuse to preferred sites for epitaxial or equiaxed growth.

An example of such a nanocrystalline, columnar microstructure is shown in Figure 5. As a consequence of this PVD microstructure, a high density of grain boundaries exists normal to the surface. It is well-known that mass transport can be greatly enhanced along grain boundaries, as compared with transport through the bulk [83]. The enhanced diffusivity of grain boundaries and the large volume fraction occupied by them was one of the key considerations in predicting nano-ionic effects [20]. Unfortunately, enhancement of ionic conductivity due to increased oxygen vacancy mobility along grain boundaries is often mitigated by space charge depletion effects, as discussed above.

Studies of cation diffusion in solid electrolytes have only recently been published for the $(La,Sr)(Ga,Mg)O_3$ [84] and zirconia systems [85]. It is well-known that the diffusivity of cations is many orders of magnitude lower that oxygen in such materials, while degradation phenomena such as creep [86] and kinetic demixing [87], are determined by the diffusion of

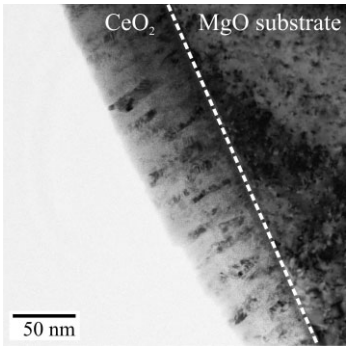

Fig. 5 Bright field TEM of a CeO_2 film grown on MgO by PLD. A columnar microstructure exists throughout the thickness of the film [82].

the slowest species. Additionally, recent reports of advanced SOFC stacks designed for intermediate temperature operation indicate that long-term stability, not electrochemical performance, may be the primary factor limiting commercialization. One such example was reported by Mai et al. in which a LSCF/GDC/YSZ stack was measured at 700 °C. The cell performance, while initially promising, decayed at a rate of 2–6% *per* 1,000 h [88]. The authors attributed this loss, in part, to the formation of a $SrZrO_3$ reaction product at the GDC/YSZ interface, indicating Sr diffusion.

Clearly, the subject of cation diffusion in solid electrolytes deserves further study, particularly in the SOFC temperature range of operation (below 1,000 °C). A simple schematic, shown in Figure 6, illustrates that a columnar-structured electrolyte provides many parallel grain boundaries, and the potential for fast diffusion into the electrolyte from the anode, cathode or both.

In-diffusion of Ni was recently investigated in nanocrystalline CeO_2 [82]; ceria films of about 1 μm thickness were deposited onto MgO substrates by PLD. As shown in Figure 5, the chosen deposition parameters resulted in nanocrystalline, columnar films. Thin NiO films of 20 nm thickness, reactively sputtered from a Ni target at room temperature, resulted in $NiO/CeO_2/MgO$ structures with low surface roughness. Typical depth profiles of ^{58}Ni, obtained by time-of-flight secondary ion mass spectrometry (TOF-SIMS) are shown in Figure 7. The shape of the profile resembles a simple error function solution to Fick's second law. After annealing at 800 °C for 5 h, the Ni penetrates through the entire CeO_2 layer and appears flat in the SIMS spectra. Diffusion of Mg from the MgO substrate was also observed. As with the case of Ni, the Mg profile resembles an error function solution to the diffusion equation.

While the vast majority of diffusion studies reported in the literature are undertaken within conditions of the Harrison regime 'B', which entails both diffusion in the bulk and along grain boundaries [89, 90], for these films, diffusion is believed to be exclusively grain boundary diffusion, thus falling under classification of the Harrison regime 'C' [26]. This is consistent with the expectation of extremely low bulk cation diffusion in fluorites at temperatures below 1,000 °C [85, 91]. For scientific studies, such boundary conditions are highly desirable, as they allow for a more straightforward and accurate determination of grain boundary diffusivities.

Following a constant source solution of the diffusion equation, grain boundary diffusivities at 700 °C of 4.6×10^{-14} and

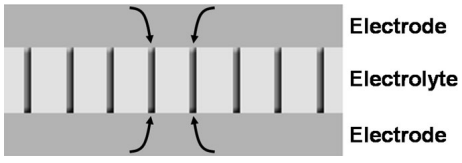

Fig. 6 Schematic cross-section of a thin film SOFC electrolyte, indicating high cross-sectional area of grain boundaries.

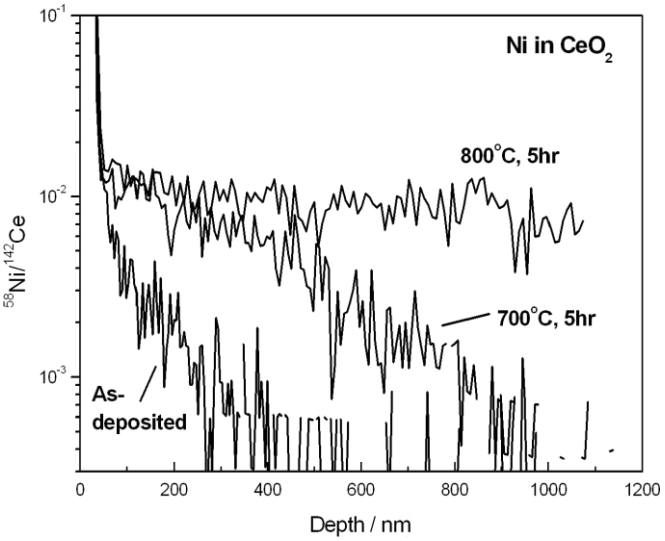

Fig. 7 SIMS spectra of ^{58}Ni diffusion in nanocrystalline CeO_2 after deposition and after annealing at 700 and 800 °C [82].

2.8×10^{-15} cm^2 s^{-1} for Ni and Mg, respectively were obtained [82]. While these values are much lower than the diffusivity of oxygen in the same temperature range, they do indicate that cations can diffuse hundreds of nanometers and even microns within hours at temperatures of 700–800 °C. To the authors' knowledge, this is the lowest temperature range for which cation grain boundary diffusion coefficients in fluorite oxides have been reported. Further research efforts to improve our understanding of cation diffusion along grain boundaries in solid electrolyte layers are currently underway.

5 Summary

In addition to power generation for large-scale applications such as housing and transportation, SOFCs also present great potential for portable power applications such as notebook computers and mobile devices. The thin-film techniques used to produce these small scale devices often lead to nanostructured electrode and electrolyte components with properties that can differ considerably from the bulk. Internal interfaces, in particular, can lead either to the enhancement [39, 41, 43] or depression [26] of ionic conductivity. Phase stability may also be altered upon nanostructuring, as shown in the case of YSZ. Nanocomposite electrodes may result in increased triple phase boundary area and reduced thermal stresses, thus enabling improvement of the electrochemical impedance of the electrode. Additionally, the high volume fraction of grain boundaries can lead to fast cation diffusion at operational SOFC temperatures [82]. Future research in this field holds the promise that such nano-ionic effects may be utilised in a systematic manner in order to improve the properties and performance of thin film SOFC components for portable power needs.

Acknowledgements

RWTH Aachen University is gratefully acknowledged for providing a Charlemagne scholarship for a student visitation by S. L. This work was supported by the National Science Foundation under award DMR-0243993 and by the Department of Defense Multidisciplinary University Research Initiative (MURI) program administered by the Army Research Office under grant no. DAAD19-01-1-0566.

List of Symbols

c_∞	Bulk defect concentration
ΔH_m	Enthalpy of migration
$\Delta\phi$	Space charge potential
ΔS_m	Entropy of migration
E	Elementary charge
ε_o	Permittivity of free space
ε_r	Relative dielectric constant
λ	Debye length
λ^*	Mott-Schottky depletion width
k	Boltzmann's constant
σ_{ion}	Partial ionic conductivity
σ_o	Temperature-independent constant
T	Temperature
zj	Charge of carrier j

References

[1] J. W. Fergus, *J. Power Sources* **2006**, *162*, 30.
[2] H. L. Tuller in *Nonstoichiometric Oxides* (Ed. O. T. Sorensen), Academic Press, New York, **1981**, pp. 271.
[3] B. C. H. Steele, A. Heinzel, *Nature* **2001**, *414*, 345.
[4] L. C. D. Baertsch, K. F. Jensen, J. L. Hertz, H. L. Tuller, S. T. Vengallatore, S. M. Spearing, M. A. Schmidt, *J. Mater. Res.* **2004**, *19*, 2604.
[5] Z. P. Shao, S. M. Haile, J. Ahn, P. D. Ronney, Z. L. Zhan, S. A. Barnett, *Nature* **2005**, *435*, 795.
[6] D. Nikbin, *The Fuel Cell Rev.* **2006**, *3*, 21.
[7] D. Beckel, A. Bierberle-Hütter, A. Harvey, A. Infortuna, U. P. Mücke, M. Prestat, J. L. M. Rupp, L. J. Gauckler, *J. Power Sources* **2007**, *173*, 325.
[8] T. Suzuki, Y. Funahashi, T. Yamaguchi, T. Fujishiro, M. Awano, *J. Power Sources* **2007**, *171*, 92.
[9] B. Chachuat, A. Mitsos, P. I. Barton, *Chem. Eng. Sci.* **2005**, *60*, 4535.
[10] S. de Souza, S. J. Visco, L. D. De Jonghe, *Solid State Ionics* **1997**, *98*, 57.
[11] A. F. Jankowski, R. T. Graff, J. P. Hayes, J. D. Morse in *Proc. 6th Int. Sym. on SOFC* (Ed., M. Dokiya, S. C. Singhal), Electrochem. Soc. Proc. 99–119, Pennington, NJ, **1999**, pp. 932.
[12] D. Perednis, L. J. Gauckler, *Solid State Ionics* **2004**, *166*, 229.
[13] A. Bieberle-Hütter, D. Beckel, A. Infortuna, U. P. Muecke, J. L. M. Rupp, L. J. Gauckler, S. Rey-Mermet, P. Muralt, N. R. Bieri, N. Hotz, M. J. Stutz, D. Poulikakos, P. Heeb, P. Müller, A. Bernard, R. Gmür, T. Hocker, *J. Power Sources* **2008**, *177*, 123.
[14] D. J. Quinn, B. Wardle, S. M. Spearing, *J. Mater. Res.* **2008**, *23*, 609.
[15] H. Huang, M. Nakamura, P. Su, R. Fasching, Y. Saito, F. B. Prinz, *J. Electrochem. Soc.* **2007**, *154*, B20.
[16] V. T. Srikar, K. T. Turner, T. Y. A. Ie, S. M. Spearing, *J. Power Sources* **2004**, *125*, 62.
[17] I. Lubomirsky, *Phys. Chem. Chem. Phys.* **2007**, *9*, 3701.
[18] A. Kossoy, Y. Feldman, E. Wachtel, I. Lubomirsky, J. Maier, *Adv. Funct. Mater.* **2007**, *17*, 2393.
[19] S. Mandowara, B. W. Sheldon, *Electrochem. Soc. Proc.* **2008**, in press.
[20] H. L. Tuller, *Solid State Ionics* **2000**, *131*, 143.
[21] J. Maier, *Solid State Ionics* **2002,** *154*, 291.
[22] J. Maier, *Solid State Ionics* **2003**, *157*, 327.
[23] J. Frenkel, *Kinetic Theory of Liquids*, Oxford University Press, New York, **1946**, pp. 7.
[24] K. Lehovec, *J. Chem. Phys.* **1953**, *21*, 1123.
[25] K. L. Kliewer, J. S. Koehler, *Phys. Rev.* **1965**, *140*, 1226.
[26] Y.-M. Chiang, E. B. Lavik, I. Kosacki, H. L. Tuller, J. Y. Ying, *J. Electroceram.* **1997**, *1*, 7.
[27] A. Tschöpe, *Solid State Ionics* **2001**, *139*, 267.
[28] S. Kim, J. Maier, *J. Electrochem. Soc.* **2002**, *149*, J73.
[29] I. Kosacki, T. Suzuki, V. Petrovsky, H. U. Anderson, *Solid State Ionics* **2000**, *136*, 1225.
[30] C. Peters, A. Weber, E. Ivers-Tiffee, H. Störmer, D. Gerthsen, M. Bockmeyer, R. Krüger, *Fall Materials Research Society (MRS) Meeting*, Boston, MA, **2006**, 712.
[31] P. Mondal, H. Hahn, Berichte der Bunsengesellschaft für Physikalische Chemie **1997**, *101*, 1765.
[32] S. Jiang, *J. Mater. Res.* **1997**, *12*, 2374.
[33] R. A. De Souza, M. J. Pietrowski, U. Anselmi-Tamburini, S. Kim, Z. A. Munir, M. Martin, *Phys. Chem. Chem. Phys.* **2008**, *10*, 2067.
[34] T. Suzuki, I. Kosacki, H. U. Anderson, P. Colomban, *J. Am. Ceram. Soc.* **2001**, *84*, 2007.
[35] T. Suzuki, I. Kosacki, H. U. Anderson, *J. Am. Ceram. Soc.* **2002**, *85*, 1492.
[36] X. Guo, J. Maier, *J. Electrochem. Soc.* **2001**, *148*, E121.
[37] S. M. Sze, *Semiconductor Devices*, Wiley & Sons, New York, **1985**, pp. 248.
[38] J. L. M. Rupp, L. J. Gauckler, *Solid State Ionics* **2006**, *177*, 2513.
[39] N. Sata, K. Eberman, K. Eberl, J. Maier, *Nature* **2000**, *408*, 2407.
[40] X. X. Guo, I. Mantei, J. Jamnik, J.-S. Lee, J. Maier, *Phys. Rev. B* **2007**, *76*, 125429.
[41] S. Azad, O. A. Marina, C. M. Wang, L. Saraf, V. Shutthanandan, D. E. McCready, A. El-Azab, J. E. Jaffe, M. H. Englehard, C. H. F. Peden, S. Thevuthasan, *App. Phys. Lett.* **2005**, *86*, 131906.

[42] C. M. Wang, M. H. Engelhard, S. Azad, L. V. Saraf, D. E. McCready, V. Shutthanandan, Z. Q. Yu, S. Thevuthasan, M. Watanabe, D. B. Williams, *Solid State Ionics* **2006**, *177*, 1299.
[43] A. Peters, C. Korte, D. Hesse, N. Zakharov, J. Janek, *Solid State Ionics* **2007**, *178*, 67.
[44] I. Kosacki, C. M. Rouleau, P. F. Becher, J. Bentley, D. H. Lowndes, *Electrochem. Solid State Lett.* **2004**, *7*, A459.
[45] I. Kosacki, C. M. Rouleau, P. F. Becher, J. Bentley, D. H. Lowndes, *Solid State Ionics* **2005**, *176*, 1319.
[46] J. B. Goodenough, *Ann. Rev. Mater. Res.* **2003**, *33*, 91.
[47] S. Hull, *Reports Prog. Phys*. **2004,** *67*, 1233.
[48] B. C. H. Steele in *High Conductivity Solid Ionic Conductors*, *Recent Trends and Applications* (Ed. T. Takahashi), World Scientific, Singapore, **1989**, pp. 402.
[49] M. Mogensen, T. Lindegaard, U. R. Hansen, G. Mogensen, *J. Electrochemic. Soc.* **1994**, *141*, 2122.
[50] M. Martin, *Zeitschrift für Physikalische Chemie* **2005**, *219*, 105.
[51] R. Garvie, *J. Phys. Chem.* **1965**, *69*, 1238.
[52] E. Djurado, P. Bouvier, G. Lucazeau, *J. Solid State Chem.* **2000**, *149*, 399.
[53] G. Baldinozzi, D. Simeone, D. Gosset, M. Dutheil, *Phys. Rev. Lett.* **2003**, *90*, 2308.
[54] J. McHale, A. Auroux, A. Perrotta, A. Navrotsky, *Science* **1987**, *277*, 788.
[55] J. Nuth, *Nature* **1978**, *329*, 589.
[56] A. S. Kao, *J. App. Phys.* **1991**, *69*, 3309.
[57] A. F. Jankowski, J. P. Hayes, *Surf. Coat. Technol.* **1995**, *76*, 126.
[58] B. Hobein, F. Tietz, D. Stover, M. Cekada, P. Panjan, *J. Eur. Ceram. Soc.* **2001**, *21*, 1843.
[59] J. L. Hertz, H. L. Tuller, *Solid State Ionics* **2007**, *178*, 915.
[60] J. Luo, D. P. Almond, R. Stevens, *J. Am. Ceram. Soc.* **2000**, *83*, 1703.
[61] M. Mogensen, S. Primdahl, M. J. Jørgensen, C. Bagger, *J. Electroceram.* **2000**, *5*, 141.
[62] F. S. Baumann, J. Fleig, H.-U. Habermaier, J. Maier, *Solid State Ionics* **2006**, *177*, 1071.
[63] A. Bieberle-Hütter, H. L. Tuller, *J. Electroceram.* **2006**, *16*, 151.
[64] A. Bieberle-Hütter, M. Soegaard, H. L. Tuller, *Solid State Ionics* **2006**, *177*, 1969.
[65] B. Abeles, P. Sheng, M. D. Coutts, Y. Arie, *Adv. Phys.* **1975**, *24*, 407.
[66] N. C. Miller, G. A. Shirn, *App. Phys. Lett.* **1967**, *10*, 86.
[67] K. Zakrzewska, M. Radecka, A. Kuk, W. Osuch, *Solid State Ionics* **2003**, *157*, 349.
[68] G. Sirinakis, R. Siddique, K. A. Dunn, H. Efstathiadis, M. A. Carpenter, A. E. Kaloyeros, L. Sun, *J. Mater. Res.* **2005**, *20*, 3320.
[69] L. S. Wang, E. S. Thiele, S. A. Barnett, *Solid State Ionics* **1992**, *52*, 261.
[70] S. A. Barnett, T. Tsai, *US Patent, US 5,656,387*, **1997**.
[71] S. A. Barnett, L. S. Wang, *US Patent, US 5,395,704*, **1995.**
[72] L. S. Wang, S. A. Barnett, *Solid State Ionics* **1995**, *76*, 103.
[73] S. A. Barnett, L. S. Wang, *US Patent, US 6,004,696*, **1999.**
[74] K. Hayashi, O. Yamamoto, Y. Nishigaki, H. Minoura, *Denki Kagaku* **1996**, *64*, 1097.
[75] K. Hayashi, O. Yamamoto, Y. Nishigaki, H. Minoura, *Solid State Ionics* **1997**, *98*, 49.
[76] U. P. Muecke, K. Akiba, A. Infortuna, T. Salkus, N. V. Stus, L. J. Gauckler, *Solid State Ionics* **2008**, *178*, 1762.
[77] U. P. Muecke, S. Graf, U. Rhyner, L. J. Gauckler, *Acta Mater.* **2008**, *56*, 677.
[78] J. E. Sundeen, R. C. Buchanan, *Sens. Actuators, A* **1997**, *63*, 33.
[79] A. M. Torres-Huerta, J. R. Vargas-Garcia, M. A. Dominguez-Crespo, *Solid State Ionics* **2007**, *178*, 1608.
[80] J. L. Hertz, H. L. Tuller, *J. Electrochem. Soc.* **2007**, *154*, B413.
[81] C. V. Thompson, *Ann. Rev. Mater. Sci.* **2000**, *30*, 159.
[82] S. J. Litzelman, R. A. De Souza, B. Butz, H. L. Tuller, M. Martin, D. Gerthsen, *J. Electroceram.* **2008**, DOI: 10.1007/s10832-008-9445-y.
[83] I. Kaur, Y. Mishin, W. Gust, *Fundamentals of Grain and Interphase Boundary Diffusion*, Wiley & Sons, West Sussex, **1995**, pp. 2.
[84] O. Schulz, M. Martin, C. Argirusis, G. Borchardt, *Phys. Chem. Chem. Phys.* **2003**, *5*, 2308.
[85] M. Kilo, *Defect and Diffusion Forum* **2005**, *242*, 185.
[86] J. Wolfenstine, *Solid State Ionics* **1999**, *126*, 293.
[87] M. Martin, *Solid State Ionics* **2000**, *136*, 331.
[88] A. Mai, M. Becker, W. Assenmacher, F. Tietz, D. Hathiramani, E. Ivers-Tiffee, D. Stöver, W. Mader, *Solid State Ionics* **2006**, *177*, 1965.
[89] L. G. Harrison, *Trans. Faraday Soc.* **1961**, *57*, 1191.
[90] A. D. LeClaire, *Br. J. App. Phys*. **1963**, *14*, 351.
[91] J. D. Sirman, D. Waller, J. A. Kilner, in *Solid Oxide Fuel Cells V* (Eds. U. Stimming, S. C. Singhal, H. Tagawa, W. Lehnert), The Electrochemical Society, Pennington, NJ, **1997**.

